Transactions on Machine Intelligence 6(3) (2023) 166-174

ISSN Online: 2821-1693

Transactions on Machine Intelligence

Journal Homepage: https://tmachineintelligence.ir/index.php/TMI

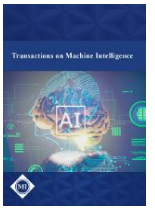

Analysis of the Process of Forming Stainless Steel Sheets Using the Forming Limit Diagram

F. Turki[1], H. Seyed Salehi[1], A. Jalali Aghchei[2,*], J. Bakhtiari Doost[1]

[1] Mechanical Engineering, K. N. Toosi University of Technology, Tehran, Iran
[2] Associate Professor, Mechanical Engineering, K. N. Toosi University of Technology, Tehran, Iran

ARTICLE INFO

Article History:
Received 5 May 2023
Received in revised form 9 July 2023
Accepted 21 September 2023
Available online 28 September 2023

Keywords:
Deep Drawing, Optimization, FLD, Sheet Forming, Forming Diagram

ABSTRACT

Formability in sheet metal forming refers to the material's ability to undergo plastic deformation without incurring defects during the manufacturing process. This typically involves shaping the metal sheet by applying force through a punch and die system, resulting in a three-dimensional deformation of the material. A key tool for evaluating formability is the Forming Limit Diagram (FLD), which graphically represents the forming limit curves. These curves illustrate combinations of major and minor strains at which localized necking also known as local throat initiation begins, thus indicating the material's plastic deformation threshold under various loading conditions. In this study, the tensile behavior of a sheet metal component was analyzed under different strain rates to assess its formability. The forming limit curve was derived through three distinct approaches: experimental testing, theoretical modeling, and finite element analysis. To support these methods, the material's work-hardening behavior was characterized using Swift's law, with its parameters determined from experimental data. The comparison of the results obtained from all three methodologies revealed a high degree of consistency, confirming the validity and reliability of the theoretical and simulation models in predicting the material's formability. These findings offer valuable guidance for improving sheet metal forming processes and minimizing failure during production.

1. INTRODUCTION

In the realm of forming processes, two primary categories stand out: volume forming and sheet forming. Among these, deep drawing emerges as a widely applied sheet forming process in various industries. It finds extensive use in crafting metal components for applications ranging from car bodies, sinks, and bathtubs to bullet casings, fuel tanks, metal beverage cans, and kitchenware [1]. Essentially, deep drawing is a tension-compression process that transforms a flat sheet into a hollow shell or modifies the dimensions of an existing hollow shell without significant changes in sheet thickness [2]. Key parameters influencing this process include sheet force, friction, die opening radius, and punch speed. A meticulous selection of these parameters is crucial to avoiding defects in the final product.

* Corresponding Author: Jalali@Kntu.ac.ir
Associate Professor, Mechanical Engineering, K. N. Toosi University of Technology, Tehran, Iran

http://dx.doi.org/10.47176/TMI.2023.166

To mitigate the risk of defects like tearing and wrinkling while simultaneously reducing production costs, computer process analysis proves invaluable. However, this demands the accurate definition of sheet properties within the software. While tensile test results provide insight into material behavior, they may fall short of capturing the complete mechanical characteristics. Incorporating the plasticity limit curve in the analysis enhances the ability to forecast sheet behavior during forming procedures. This curve illustrates the necking moment across different strain fields, and if the material's strain state surpasses the curve, failure is imminent, as illustrated in Figure 1, depicting the limit of formability (FLD) curve and its distinct sections. A thorough understanding of the material's state is attainable by examining the specific region on the FLD curve corresponding to the strain state [3].

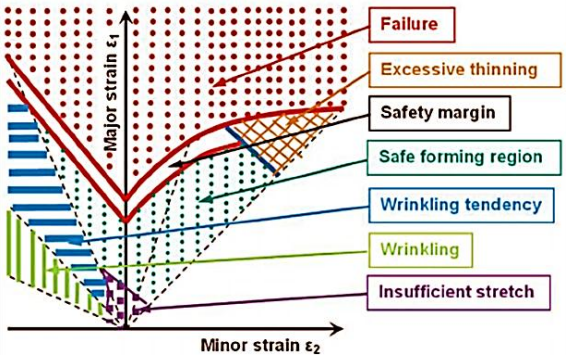

Fig. 1. Formability limit curve and interpretation of its different areas

To establish the plasticity limit curve of a sheet, researchers have employed various tests such as the Nakajima and Marciniak tests. In both methods, specialized tools are utilized to deform the sheet until the point of throating, and the measurement of main strains in the throating area is then conducted [4]. Deep drawing processes are broadly categorized as rotating or non-rotating, depending on the geometry of the resulting product. Deep drawing research has commonly focused on processes yielding a rotating geometry, specifically cylindrical or conical shapes. In 2007, Oliveiraa et al. delved into the impact of process parameters on the deep drawing of stainless steel, providing valuable insights. They quantified the influence ratio of three critical deep drawing process parameters - the edge radius of the die, force of the plate holder, and coefficient of friction - using the finite element method. The study revealed that the die radius at 2.89% had a primary influence on deep drawing, while the coefficient of friction and force of the sheet holder contributed by 6.3% and 4.5%, respectively [5].

In 2011, Ravindra et al. conducted a study employing numerical failure analysis to predict failure initiation in deep tension. The investigation indicated that the maximum cup height, where the cup tears, increases with thicker sheet thickness, a larger edge radius of the punch, and a larger radius of the die. The initiation of fracture in a circular cup is significantly impacted by the plastic properties, including the initial yield stress and strain-hardening parameter, while in a square cup, failure initiation is primarily influenced by plastic deformation in the corner region due to the presence of corners [6].

Gwasa and Izsiler conducted research to investigate the impact of plate holder distance on the deep drawing process [7]. Their experiments analyzed distances ranging from 1 to 1.9 mm for 1 mm thick aluminum sheets. The findings highlight that the optimal distance of the sheet holder significantly influences the quality of the final part. Increasing the sheet holder distance allows more material to be drawn into the die cavity without causing damage or resulting in an abnormal shape. However, a significantly larger sheet gap may lead to increased wrinkling, twisting in straight walls, and tearing. The study determined that the optimal forming quality lies in the range of 1 to 1.3 mm [7]. In 2011, Ozek et al. explored the impact of die angle, plate holder angle, and punch and die edge radii on the tensile limit ratio, punch force, and minimum wall thickness of a steel sheet during the deep drawing of angular square sections [8]. They observed that varying these variables influenced the quality of the final product. Experimental data was collected, and statistical analysis of variance was employed to assess the impact of these variables on the tensile limit ratio, punch force, and minimum sheet wall thickness. The experiments involved the creation of four dies and sheet holders machined to include angles of 0, 5, 10, and 15 degrees, along with punch and

die edge radii of 8, 12, and 16 mm. The results indicate that as the angle and radius of the die and punch increase, the tension ratio also increases [8].

In 2014, Boissiere and collaborators conducted research on the influence of punch geometry and dimensions on the forming limit diagram during deep drawing using aluminum 2024 alloy. Their study focused on two types of punch heads, flat and spherical, in varying sizes measured in both centimeters and decimeters. The findings revealed that the flat punch head had a more pronounced effect on the process. The punch, consisting of flat and spherical heads, was examined in two different sizes measured in decimeters and centimeters. Results demonstrated that the spherical head mandrel achieved a greater depth of tension compared to the flat head punch. Moreover, the spherical head punch exhibited less sensitivity to size scale variations than its flat head counterpart [9].

Wu et al. (2019) conducted a study on the forming process, microstructure, and mechanical properties of thin-walled 316L stainless steel using speed-cold-welding additive manufacturing. Their research focused on the manufacturing process and the resulting mechanical properties. The findings of this study would be valuable in understanding the behavior of stainless steel sheets during the forming process. However, the study did not specifically delve into the forming limit diagram of stainless steel, which is a crucial aspect of the forming process [10]. In another study, Sirirerkratana et al. (2019) investigated the use of stainless steel sheets in the photocatalytic process for color removal from wastewater. Although this study did not directly address the forming process, it highlighted a potential application of stainless steel sheets in environmental processes. This suggests that there is a need for further research to explore the impact of the forming process on the properties of stainless steel sheets in specialized applications such as wastewater treatment [11].

Vahdani et al. (2019) explored the electric hot incremental sheet forming of various materials, including DC01 steel sheets. The findings of this study shed light on the incremental forming process, which is relevant to the understanding of the forming limit diagram for stainless steel sheets. By comparing the behavior of different materials during the forming process, this study provides insights that can contribute to the understanding of the formability of stainless steel sheets [12]. Furthermore, Trzepieciński (2019) conducted a study on the coefficient of friction in steel sheets forming. While this study did not specifically focus on stainless steel, the findings related to the frictional behavior of steel sheets are relevant to the understanding of the forming process. Friction is a critical factor in sheet metal forming, and further research on the frictional behavior of stainless steel sheets would contribute to a comprehensive understanding of the forming process [13].

Leng, Ming, Yang, and Zhang (2020) investigated the use of stainless steel bipolar plates for proton exchange membrane fuel cells. The study focused on the materials, flow channel design, and forming processes. The findings of this study underscore the significance of understanding the mechanical behavior and forming limits of stainless steel in the context of fuel cell applications, thus emphasizing the relevance of the forming limit diagram in optimizing the forming processes for such applications [14].

Kotkunde, Krishna, Shenoy, Gupta, and Singh (2017) conducted experimental and theoretical investigations of the forming limit diagram for Ti-6Al-4 V alloy at warm conditions. Although the study focused on a different material, the insights gained from this research can be extrapolated to the analysis of stainless steel sheets [15]. Understanding the formability characteristics of different materials, including stainless steel, is essential for developing accurate and reliable forming limit diagrams that can aid in the optimization of the forming processes.

In a study by Lambiase and Genna (2017), the laser-assisted direct joining of AISI304 stainless steel with polycarbonate sheets was investigated. The research involved thermal analysis, mechanical characterization, and bonds morphology. While the focus of this study was on joining processes, the findings are relevant to the understanding of the formability of stainless steel sheets, especially in the context of laser-assisted forming processes. The integration of laser technology with the forming process has the potential to influence the material behavior and formability, thereby necessitating a comprehensive analysis using the forming limit diagram [16].

Wu, Xue, Wang, Zhang, Hu, and Dong (2019) explored the forming process, microstructure, and mechanical properties of thin-walled 316L stainless steel using speed-cold-welding additive manufacturing. This study provided insights into the influence of the forming process on the microstructure and mechanical properties of stainless steel. The utilization of advanced manufacturing techniques such as additive manufacturing further emphasizes the need

for an in-depth understanding of the formability of stainless steel sheets, which can be effectively achieved through the analysis of the forming limit diagram [17].

This investigation delves into the parameters influencing the deep drawing process of a rectangular cross-section cup. The primary objective is to explore the impact of process and geometric parameters and determine the optimal conditions for achieving the maximum depth of stretching in the final product. While increasing the number of drawing steps and implementing heat treatment for each step may result in a higher drawing depth, the associated costs are significantly elevated. Additionally, the use of heat treatment may introduce undesirable negative effects on the metal's chemical properties, such as resistance to oxidation and corrosion.

2. EXPERIMENT PROCEDURE

The material of this article is a St304 sheet with a thickness of 0.8 mm. The chemical composition of the steel used, according to Table 1.

Table 1. Chemical composition of stainless steel 304

C	Si	Mn	P	S	Cr	Fe
0.045	0.39	1.05	0.026	<0.005	17.73	**Base**
Mo	Ni	Al	Co	Cu	Nb	
0.09	8.25	0.005	0.19	0.21	0.03	
Ti	V	W	Pb	Sn	Se	
0.007	**0.09**	**0.03**	**<0.01**	**0.01**	**<0.005**	

To acquire the mechanical properties of the desired sheet, uniaxial tension tests were employed to extract anisotropy coefficients and analyze the material's plasticity behavior at different speeds. Additionally, a stretch test using a spherical head punch (Nakajima test) was conducted to extract the ductility limit curve. The tensile tests were carried out following the ASTM E8/E8M standard, while the stretch test with a spherical punch adhered to the ISO 12004-2-2008 standard. Laser engraving measurement, employing the Circle Grid Analysis method (Fig. 2), was utilized to measure limit strains.

Fig. 2. A sample of fiber laser engraving

The nominal outer diameter of the circles is 5 mm and their nominal inner diameter is 4 mm. Tensile test at three speeds of 2.5, 126.25 and 250 mm/min for displacement rate and each is repeated twice. (6 tests in total). In Fig. 3., samples drawn at different speeds are seen.

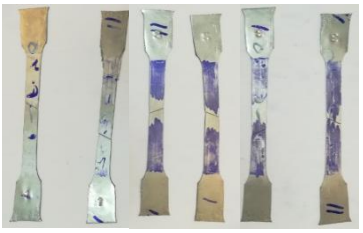

Fig. 3. samples for tensile test

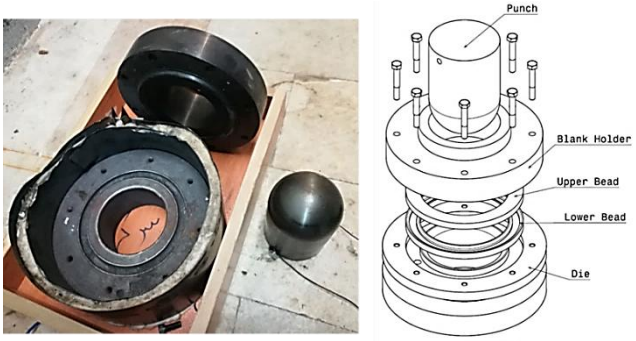

Fig. 4. Die used for FLD test

At Fig. 4., the die and punch that used in the stretch test is shown. The test procedure involves placing the sample on the matrix, securing the sheet holder to the matrix by tightening the screws. Subsequently, to generate the sheet removal force, the assembly is positioned under the press, and the ram press exerts downward pressure on the sheet holder until the designated force is achieved. Following this, while keeping the ram press stationary, the previously loosened sheet-holding screws are tightened to a torque of 5 N.m with the aid of a torque meter.

2.1. The procedure of experiment validation

AutoForm is a versatile software dedicated to die design and analysis, automating the meshing process for designated dies. It adheres to strict grammatical correctness and follows a structured approach, limiting each element to a maximum chord size of 10mm. Within the Process section of the PL branch, specific friction conditions and Coulomb friction coefficients between identical components are defined to achieve desired values. The punch and die are assumed to be rigid, while the sheet holder is considered an elastic body.

In the Simulation section, parameters related to sheet meshing are adjustable within the Control branch. All analyses employ the exact FV mode to comprehensively consider the engineering phase. Customizable settings for this problem encompass radial penetration, maximum element angle, and initial element size. A shell-type element with 11 integral points along the thickness (EPS-11) is employed, and the problem is analyzed as plane stress. The meshing and assembly of the mold parts are visually depicted in Fig. 5.

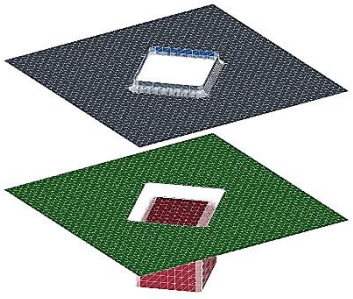

Fig. 5. Meshing and assembly of mold components

3. RESULTS

Preparation of the true stress diagram in terms of true strain was drawn according to Fig. 6. Consistency in the strain-hardness power values is ideally achieved across all tests. The experimental explanations indicate that curve fitting to the strain of the data limits resulted in strain-hardness power values ranging from 0.51 to 0.68. In the gauge area of the process, once a specific strain is reached, stress in the jaw area surpasses the yield value, leading to material flow in that region. During the curve fitting in MATLAB, data exceeding strains of 0.2 were excluded. The SWIFT strain-hardness coefficients are depicted by a power curve fitted on this graph, utilizing the curve fitting tool in MATLAB software. Figure 7 visually represents the curve fitting space in MATLAB, with the red-colored parts of the graph indicating the excluded points.

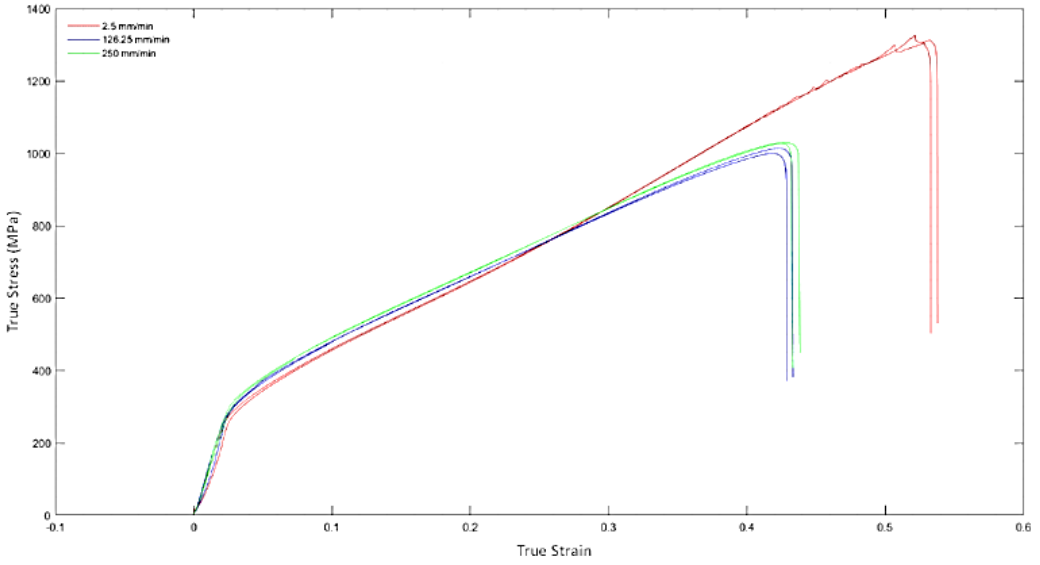

Fig. 6. True stress and true strain obtain from tensile test

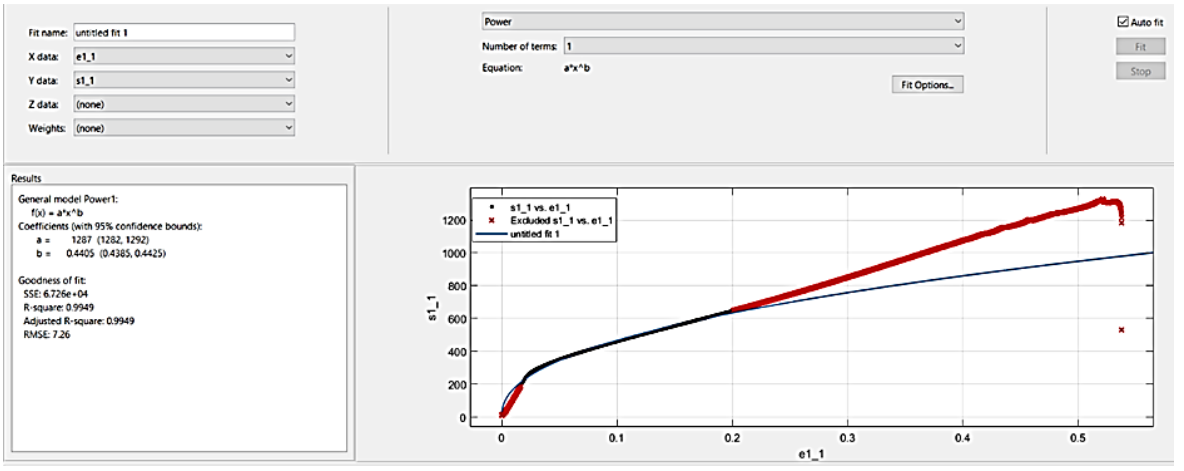

Fig. 7. Curve fitting environment in MATLAB

The a and b values provided by the software for the data set are actually the same as C and m in the Swift equation. Since the material used is not pre-hardened, ε_0 actually represents the strain at which the material reaches the yield point. This value is considered equal to 0.0241 by reading the graphs drawn from the test data in Fig. 6. Table 2 shows the values of c and m coefficients obtained from fitting the curve on the graphs. In order to obtain the power of sensitivity to the strain rate, one should use the part of the diagram in Fig. 6. where the stress at the same strain is

larger for higher speeds, and this is the case until the strain is about 0.22. Table 3 shows the Data used to calculate strain rate sensitivity.

Table 2. Coefficients obtained from curve fitting on graphs

m	C	Jaw movement speed (mm/min)	Number of experiments
0.4405	1287	2.5	**1**
0.4560	1316	2.5	**2**
0.4168	1269	126.25	**3**
0.4274	1295	126.25	**4**
0.4274	1305	250	**5**
0.4212	1270	250	**6**

Table 3. Data used to calculate strain rate sensitivity

Strain rate (1/s)	Average true stress (Mpa)	True strain	Jaw movement speed (mm/min)
0.0005	645	0.2	2.5
0.02525	659		126.25
0.05	671.5		250

Then, the average true stresses are drawn in terms of strain rate, and like what was done to find C and m, the sensitivity power to strain rate (a) is obtained as 0.007713. The speed of 2.5 mm/min is considered as a reference. The final equation that uses is stated in Eq. 1.

$$\sigma = C\left(\varepsilon_{pl} + \varepsilon_0\right)^m . \left(\frac{\dot{\varepsilon}}{\dot{\varepsilon}_{ref}}\right)^a = 1287 \times \left(0.0241 + \varepsilon_{pl}\right)^{0.4405} \times \left(\frac{\dot{\varepsilon}}{0.0005}\right)^{0.007713} \quad (1)$$

In Fig. 8., the strains measured to obtain the experimental FLD are compared with the existing theoretical FLDs from different methods.

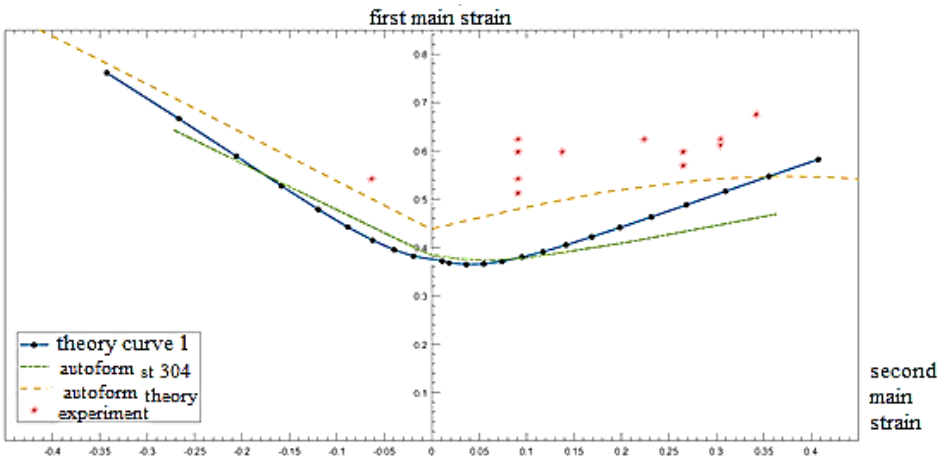

Fig. 8. Theoretical, experimental and Auto form plasticity limit curves, related to the desired material

The measured points surpass the theoretical curves. Strains above 0.2 were disregarded during curve fitting to extract the strain-hardness properties of the material. Including the entire strain range in the fitting process would lead to increased coefficients, altering the inputs for extracting theoretical curves. Conversely, as the hardness strain power (n) in the Holoman relation increases, ductility also increases. Higher ductility results in a raised FLD curve. Therefore, fitting coefficients over the entire strain range and inputting them to the theoretical FLD problem causes the curves to become higher and approach experimental data. Careful selection led to choosing the blue curve.

To ensure accurate results from the finite element and verify the extracted material information, the experiment's process was simulated in the software and compared with the results. Thickness distribution on an industrial product that underwent deep drawing was examined as an output parameter between finite element analysis and experience. To determine the real sample's thickness, a wire cutter was used to create a piece, and measurements were taken at

2 cm intervals along a specific path. The corresponding thickness in the finite element at the same points was then extracted and compared.

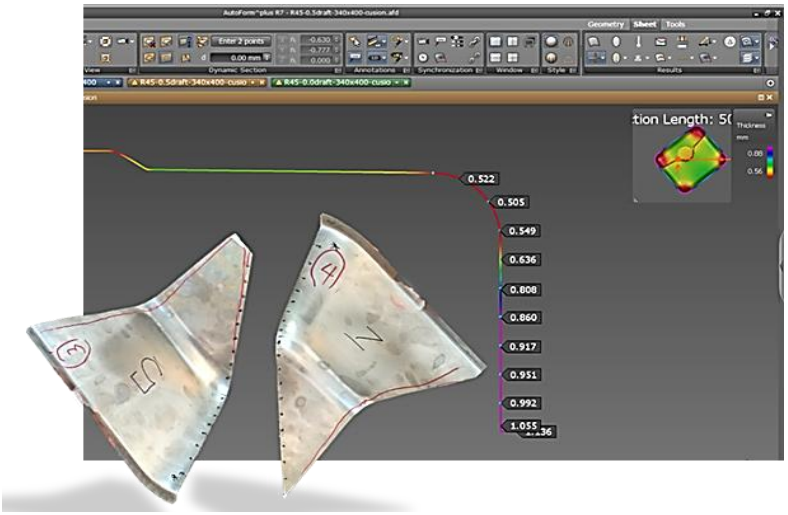

Fig. 9. obtaining the thickness in the path determined in the software

The average relative error measured between finite element and experiment was calculated as 11.8%. This error reaches its maximum in the flange area and its minimum value of about 3% in the three corners of the product.

4. CONCLUSION

In this article:

- First, by performing uniaxial tensile tests at different speeds and expansion tests with a mandrel, the ductility properties have been extracted. These properties include the coefficients related to the Swift strain-hardness relationship and the plasticity limit curve of the material.
- By extracting the forming and ductility properties of a sheet of 304 stainless steel, the finite element investigation of the forming properties of deep drawing in the deep drawing process of a cup with a rectangular cross-section was investigated.
- By comparing experimental results with finite element, the depth of stretching before entering the zone of excessive thinning, the value of 42.94 mm has been obtained and it is 1% different from the predicted value.
- By comparing the experimental and numerical results at most points, the finite element shows a higher value for the thickness. It can be seen that the Autoform software provides the thickness of the product in the wrinkling area with a large error, but on the other hand, in the critical areas of the piece, which are the corners, it can predict the result with high accuracy.

CONFLICTS OF INTEREST

The authors declare no conflict of interest.

REFERENCES

[1] Yoon, S. J., & Yang, D. Y. (2005). An incremental roll forming process for manufacturing doubly curved sheets from general quadrilateral sheet blanks with enhanced process features. CIRP annals, 54(1), 221-224.

[2] Colgan, M., & Monaghan, J. (2003). Deep drawing process: analysis and experiment. Journal of Materials Processing Technology, 132(1–3), 35–41. doi:10.1016/s0924-0136(02)00253-

[3] Paul, S. K. (2013). Theoretical analysis of strain-and stress-based forming limit diagrams. The Journal of Strain Analysis for Engineering Design, 48(3), 177–188.

[4] Wankhede, P., & Suresh, K. (2020). A review on the evaluation of formability in sheet metal forming. Advances in Materials and Processing Technologies, 6(2), 458–485. doi:10.1080/2374068x.2020.1731229

[5] Padmanabhan, R., Oliveira, M. C., Alves, J. L., & Menezes, L. F. (2007). Influence of process parameters on the deep drawing of stainless steel. Finite Elements in Analysis and Design: The International Journal of Applied Finite Elements and Computer Aided Engineering, 43(14), 1062–1067. doi:10.1016/j.finel.2007.06.011

[6] Saxena, R. K., & Dixit, P. M. (2011). Numerical analysis of damage for prediction of fracture initiation in deep drawing. Finite Elements in Analysis and Design: The International Journal of Applied Finite Elements and Computer Aided Engineering, 47(9), 1104–1117. doi:10.1016/j.finel.2011.04.003

[7] Gavas, M., & Izciler, M. (2007). Effect of blank holder gap on deep drawing of square cups. Materials in Engineering, 28(5), 1641–1646. doi:10.1016/j.matdes.2006.03.024

[8] Özek, C., & Ünal, E. (2011). Optimization and modeling of angular deep drawing process for square cups. Materials and Manufacturing Processes, 26(9), 1117–1125. doi:10.1080/10426914.2010.532526

[9] Boissiere, R., Vacher, P., & Blandin, J. J. (2014). Scale factor and punch shape effects on the expansion capacities of an aluminum alloy during deep-drawing operations. Mechanics & Industry, 15(2), 159–166. doi:10.1051/meca/2014015

[10] Wu, Wei., Xue, J.., Wang, Leilei., Zhang, Zhanhui., Hu, Yu., & Dong, C.. (2019). Forming Process, Microstructure, and Mechanical Properties of Thin-Walled 316L Stainless Steel Using Speed-Cold-Welding Additive Manufacturing. *Metals* . http://doi.org/10.3390/MET9010109

[11] Sirirerkratana, Krit., Kemacheevakul, Patiya., Kemacheevakul, Patiya., & Chuangchote, S.. (2019). Color removal from wastewater by photocatalytic process using titanium dioxide-coated glass, ceramic tile, and stainless steel sheets. *Journal of Cleaner Production* . http://doi.org/10.1016/J.JCLEPRO.2019.01.037

[12] Vahdani, Mostafa., Mirnia, M. J.., Bakhshi-Jooybari, M.., & Gorji, H.. (2019). Electric hot incremental sheet forming of Ti-6Al-4V titanium, AA6061 aluminum, and DC01 steel sheets. *The International Journal of Advanced Manufacturing Technology* , 1-11 . http://doi.org/10.1007/S00170-019-03624-2

[13] Trzepieciński, T.. (2019). A Study of the Coefficient of Friction in Steel Sheets Forming. *Metals* . http://doi.org/10.3390/met9090988

[14] Leng, Y.., Ming, P.., Yang, Daijun., & Zhang, Cunman. (2020). Stainless steel bipolar plates for proton exchange membrane fuel cells: Materials, flow channel design and forming processes. *Journal of Power Sources* , 451 , 227783 . http://doi.org/10.1016/j.jpowsour.2020.227783

[15] Kotkunde, N.., Krishna, G.., Shenoy, S.., Gupta, A.., & Singh, Swadesh Kumar. (2017). Experimental and theoretical investigation of forming limit diagram for Ti-6Al-4 V alloy at warm condition. *International Journal of Material Forming* , 10 , 255-266 . http://doi.org/10.1007/S12289-015-1274-3

[16] Lambiase, F.., & Genna, S.. (2017). Laser-assisted direct joining of AISI304 stainless steel with polycarbonate sheets: Thermal analysis, mechanical characterization, and bonds morphology. *Optics and Laser Technology* , 88 , 205-214 . http://doi.org/10.1016/J.OPTLASTEC.2016.09.028

[17] Wu, Wei., Xue, J.., Wang, Leilei., Zhang, Zhanhui., Hu, Yu., & Dong, C.. (2019). Forming Process, Microstructure, and Mechanical Properties of Thin-Walled 316L Stainless Steel Using Speed-Cold-Welding Additive Manufacturing. *Metals* . http://doi.org/10.3390/MET9010109